Supplemental Material: Topological phase transition induced by $p_{x,y}$ and p_z band inversion in honeycomb lattice

Huisheng Zhang,[*a,b] Yaohui Ning,[a] Wenjia Yang,[a] Ruiqiang Zhang[a] and Xiaohong Xu[*a]

[a]*Key Laboratory of Magnetic Molecules and Magnetic Information Materials of the Ministry of Education, Research Institute of Materials Science, and College of Physics and Electronic Information, Shanxi Normal University, Linfen 041004, China. Email: hszhang@sxnu.edu.cn,xuxh@sxnu.edu.cn*

[b]*State Key Laboratory of Surface Physics and Department of Physics, Fudan University, Shanghai 200433, China.*

Supplementary Note 1

In the basis of three-orbitals TB model for a honeycomb lattice with two $p_{x,y}$ orbitals on A site and one p_z orbital on B site, the Hamiltonial $H(k)$ with a 3 × 3 matrix can be written as

$$H_{hop}(k)=\sum_{\alpha}\varepsilon_{\alpha}c_{0\alpha}^{+}c_{0\alpha}+\sum_{i}\sum_{\alpha,\beta}(t_{0\alpha,i\beta}c_{0\alpha}^{+}c_{i\beta}+t_{i\beta}c_{i\beta}^{+}c_{0\alpha}), \quad (1)$$

where $\alpha,\beta=p_x,p_y,p_z$ are the orbital index, ε_{α} is the on-site energy and $t_{0\alpha,i\beta}$ is the nearest-neighbor (NN) hopping parameter. c^{+} and c are creation and annihilation operators. The detailed 3 × 3 matrix elements without consideration of SOC are

$$\begin{aligned}
H_{11}&=\varepsilon_{px}+2\cos\sqrt{3}k_yV_{pp\pi}+\left(\frac{3}{2}V_{pp\sigma}+\frac{1}{2}V_{pp\pi}\right)\times\left[\cos\left(\frac{3}{2}k_x+\frac{\sqrt{3}}{2}k_y\right)+\cos\left(\frac{3}{2}k_x-\frac{\sqrt{3}}{2}k_y\right)\right],\\
H_{12}&=\frac{\sqrt{3}}{2}\left(V_{pp\sigma}-V_{pp\pi}\right)\times\left[\cos\left(\frac{3}{2}k_x+\frac{\sqrt{3}}{2}k_y\right)-\cos\left(\frac{3}{2}k_x-\frac{\sqrt{3}}{2}k_y\right)\right],\\
H_{13}&=\frac{1}{2}\left(V_{pp\sigma}-V_{pp\pi}\right)\times\left[e^{ik_x}-e^{-\frac{i}{2}k_x}\times\cos\frac{\sqrt{3}}{2}k_y\right],\\
H_{22}&=\varepsilon_{py}+2\cos\sqrt{3}k_yV_{pp\sigma}+\left(\frac{1}{2}V_{pp\sigma}+\frac{3}{2}V_{pp\pi}\right)\times\left[\cos\left(\frac{3}{2}k_x+\frac{\sqrt{3}}{2}k_y\right)+\cos\left(\frac{3}{2}k_x-\frac{\sqrt{3}}{2}k_y\right)\right],\\
H_{23}&=\frac{\sqrt{3}}{2}i\left(V_{pp\sigma}-V_{pp\pi}\right)\times e^{-\frac{i}{2}k_x}\times\sin\frac{\sqrt{3}}{2}k_y,\\
H_{33}&=\varepsilon_{pz}+2\cos\sqrt{3}k_yV_{pp\pi}+2V_{pp\pi}\times\left[\cos\left(\frac{3}{2}k_x+\frac{\sqrt{3}}{2}k_y\right)+\cos\left(\frac{3}{2}k_x-\frac{\sqrt{3}}{2}k_y\right)\right],\\
H_{21}&=H_{12}^{*},H_{32}=H_{23}^{*},H_{31}=H_{13}^{*}.
\end{aligned} \quad (2)$$

where ε_{px}, ε_{py}, and ε_{pz} are on-site energies for p_x, p_y, and p_z orbitals, respectively. $V_{pp\sigma}$ and $V_{pp\pi}$ are NN hopping parameters. The bulking distance h equals to the bond length between A and B sites. Around the Γ point, the above Hamiltonian can be expended to the first-order of k as

$$H_{hop}(k)=\begin{bmatrix} \varepsilon_{px}+3(V_{pp\sigma}+V_{pp\pi}) & 0 & \frac{3}{4}ik_x(V_{pp\sigma}-V_{pp\pi}) \\ 0 & \varepsilon_{py}+3(V_{pp\sigma}+V_{pp\pi}) & \frac{3}{4}ik_y(V_{pp\sigma}-V_{pp\pi}) \\ -\frac{3}{4}ik_x(V_{pp\sigma}-V_{pp\pi}) & -\frac{3}{4}ik_y(V_{pp\sigma}-V_{pp\pi}) & \varepsilon_{pz}+6V_{pp\pi} \end{bmatrix}, \quad (3)$$

Since the on-site SOC term does not induce the coupling between different spin components, i.e., the spin-up and spin-down spaces are separated, it can be written as

$$H_{SOC\uparrow/\downarrow}=s\cdot\lambda_{SOC}\begin{bmatrix} 0 & -i & 0 \\ i & 0 & 0 \\ 0 & 0 & 0 \end{bmatrix}, \quad (4)$$

where λ_{SOC} is the atomic SOC strength, and $s=\pm1$ represent spin-up and spin-down components, respectively. Hence, the total spin-up Hamiltonian $H(k)$ with consideration of SOC is

$$H(k)=H_{hop}(k)+H_{SOC}=\begin{bmatrix} \varepsilon_{px}+3(V_{pp\sigma}+V_{pp\pi}) & 0 & \frac{3}{4}ik_x(V_{pp\sigma}-V_{pp\pi}) \\ 0 & \varepsilon_{py}+3(V_{pp\sigma}+V_{pp\pi}) & \frac{3}{4}ik_y(V_{pp\sigma}-V_{pp\pi}) \\ -\frac{3}{4}ik_x(V_{pp\sigma}-V_{pp\pi}) & -\frac{3}{4}ik_y(V_{pp\sigma}-V_{pp\pi}) & \varepsilon_{pz}+6V_{pp\pi} \end{bmatrix}, \quad (5)$$

Supplementary Note 2

In the three-orbitals TB model, the buckling distance h (Figure 1(a)) equals to the bond length a between A and B sites. Here, we have systematically investigated the nontrivial bandgaps as the function of h, where, $h = xa$ (x = 0.0-2.0), the detailed 3 × 3 matrix elements without consideration of SOC are the same as equation (2), except that

$$
\begin{aligned}
H_{13} &= \frac{x}{x^2+1}\left(V_{pp\sigma} - V_{pp\pi}\right)\times\left[e^{ik_x} - e^{-\frac{i}{2}k_x}\times\cos\frac{\sqrt{3}}{2}k_y\right], \\
H_{23} &= \frac{\sqrt{3}x}{x^2+1}i\left(V_{pp\sigma} - V_{pp\pi}\right)\times e^{-\frac{i}{2}k_x}\times\sin\frac{\sqrt{3}}{2}k_y, \\
H_{31} &= H_{13}^*, H_{32} = H_{23}^*.
\end{aligned} \tag{6}
$$

As displayed in Fig. S1, the bandgap rapidly increases from zero, and reaches its maximum when $h = a$, then slowly decreases with h increasing. And five typical band structures with h = 0.0, 0.1, 0.5, 1.0, and 1.5 are also shown, respectively. When h = 0.0, $H_{13} = H_{23} = H_{23} = H_{32} = 0$, which means that the coupling between $p_{x,y}$ and p_z orbitals is zero. In this case, the bandgap can not be opened, as shown in Fig. S1(b). As h represents the distance between two atoms, the chosen value can not be too large.

Supplementary Note 3

The thermodynamic stability of Si_2I/MgI_2 heterostructure were performing in *ab initio* molecular dynamics (AIMD) simulations at 200 K. In the simulations, we have used 4 × 4 × 1 supercell for the heterostructure, to allow the systems to be reconstructed freely at the given temperature. Here, a canonical ensembles (NVT) was adopted for the AIMD simulations by using the algorithm of Nosé (S. Nosé, *J. Chem. Phys.*, 1984, **81,** 511), with the time step of 2 fs. After 20 ps AIMD simulations, Si_2I/MgI_2 heterostructure preserve their respective structures as shown in Fig. S7, indicating their thermodynamic stability at 200 K.

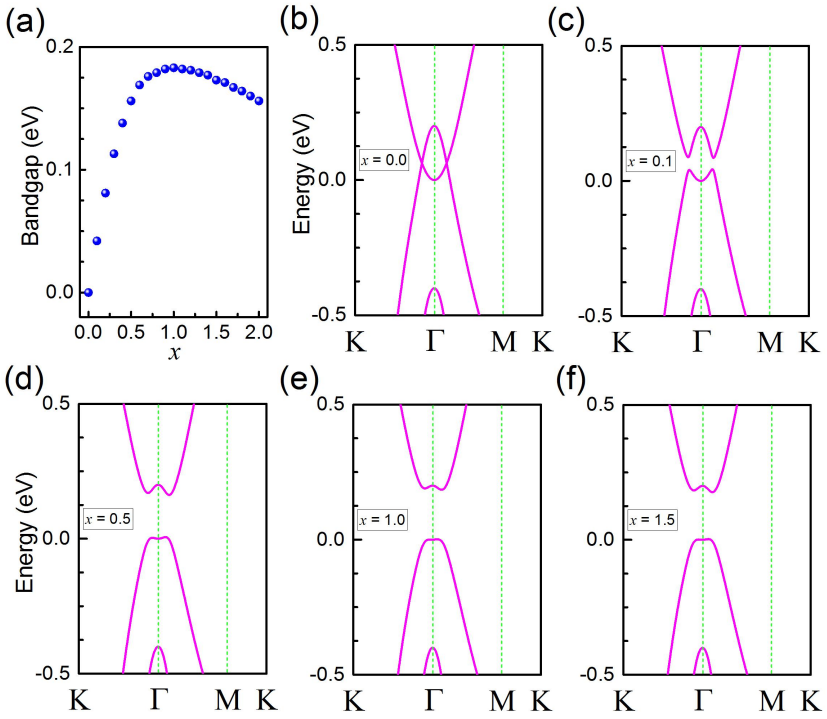

Fig. S1 (a) The nontrivial bandgaps as the function of h. (b)-(f) The calculated band structures with h = 0.0, 0.1, 0.5, 1.0, and 1.5, respectively. Here, the parameters are set to $\varepsilon_{px} = \varepsilon_{py}$ = -1.6 eV , ε_{pz} = 0.6 eV, $V_{pp\pi}$ = -0.1 eV,$V_{pp\sigma}$ = 0.6 eV. λ_{SOC} is 0, 0.1, and 0.3 eV for all cases. Fermi level is set to zero.

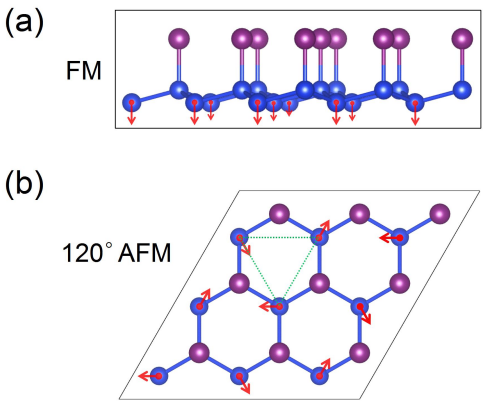

Fig. S2 Ferromagnetic (a) and 120° antiferromagnetic (b) orders of freestanding Si_2I in 3×3 unit cell. The green dashed lines denote that nearest three "magnetic" atoms form 120° antiferromagnetic order.

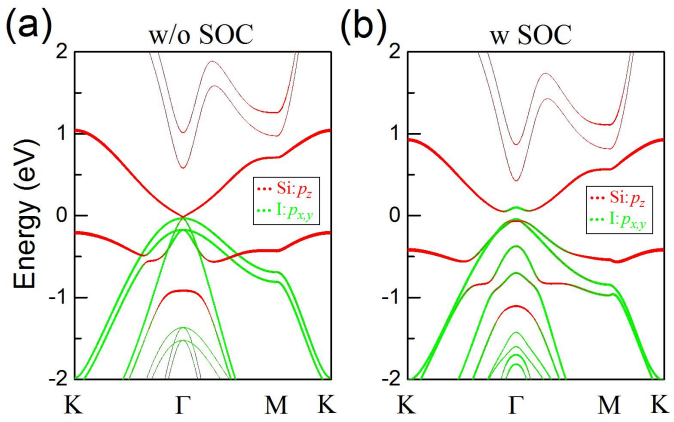

Fig. S3 Projected band structures of freestanding Si_2I without (a) and with (b) consideration of SOC. Here, red and green colors represent weight of Si p_z and I $p_{x,y}$ orbitals, respectively. Obviously, a band inversion happens near Fermi level between Si p_z and I $p_{x,y}$ when SOC is applied.

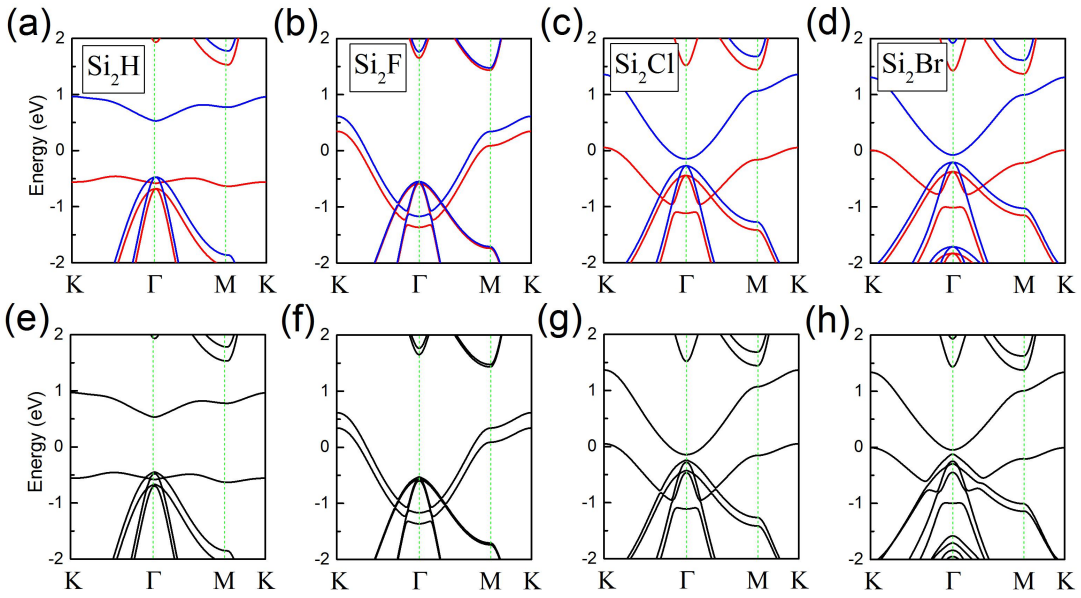

Fig. S4 Band structures of freestanding Si_2X (X = H, F-Br) without ((a)-(d)) and with ((e)-(h)) consideration of SOC, respectively.

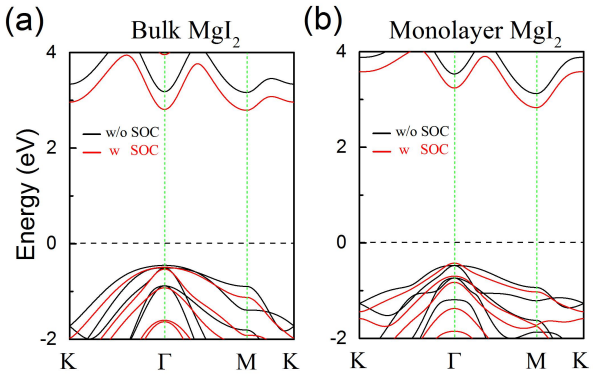

Fig. S5 Band structure of bulk (a) and monolayer (b) MgI_2 without (black lines) and with (red lines) SOC. The black dashed lines indicate Fermi level.

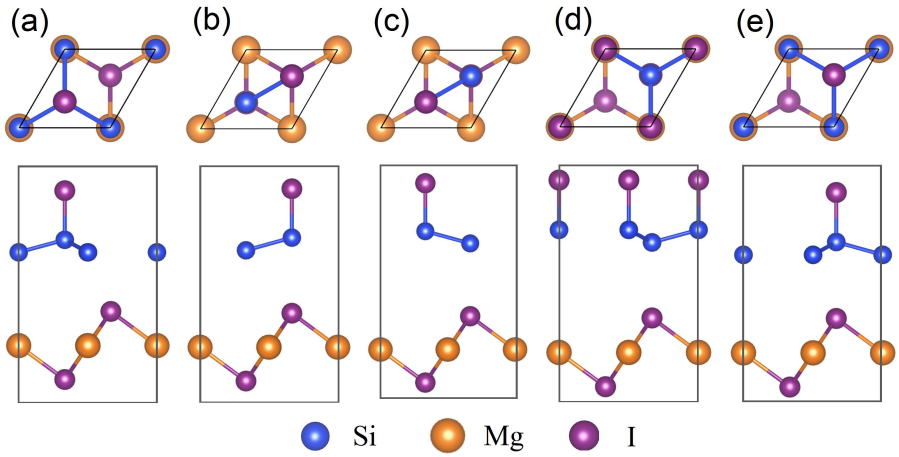

Fig. S6 The other five high-symmetry stacking configurations of Si_2I/MgI_2 heterostructures in a 1×1 unit cell.

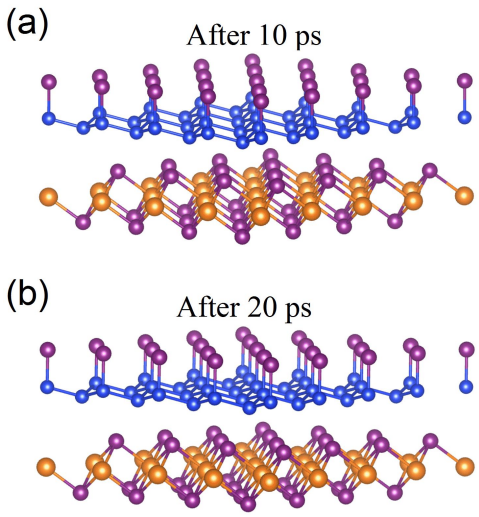

Fig. S7 Schematic diagram of Si_2I/MgI_2 heterostructures after 10 (a) and 20 (b) ps of AIMD simulations.

Table S1. The bandgaps of three systems (Si_2I, Si_2I/MgI_2,Bi/Si(111)) calculated with four typical vdW functionals.

		Functional			
		DFT-D2	vdW-DF	optPBE-vdW	vdW-DF2
E_g (eV)	Si_2I	0.094	0.094	0.094	0.094
	Si_2I/MgI_2	0.093	0.094	0.095	0.095
	Bi/Si(111)	0.060	0.060	0.060	0.060